



Published in final edited form as:

*J Am Chem Soc.* 2016 December 07; 138(48): 15551–15554. doi:10.1021/jacs.6b10538.

## Helix-dependent Spin Filtering through the DNA Duplex

Theodore J. Zwang<sup>1</sup>, Sylvia Hurlimann<sup>1</sup>, Michael G. Hill<sup>2</sup>, and Jacques-line K. Barton<sup>1,\*</sup>

<sup>1</sup>Division of Chemistry and Chemical Engineering, California Institute of Technology, Pasadena, CA 91125

<sup>2</sup>Division of Chemistry, Occidental College, Los Angeles, CA, 90041

### Abstract

Recent work suggests that electrons can travel through DNA and other chiral molecules in a spin-selective manner, but little is known about the origin of this spin selectivity. Here we describe experiments on magnetized DNA-modified electrodes to explore spin-selective electron transport through hydrated duplex DNA. Our results show that the two spins migrate through duplex DNA with different yield, and that spin selectivity requires charge transport *through* the DNA duplex. Significantly, shifting the same duplex DNA between right-handed B- and left-handed Z-forms leads to a diode-like switch in spin-selectivity; which spin moves more efficiently through the duplex depends upon the DNA helicity. With DNA, the supramolecular organization of chiral moieties, rather than the chirality of the individual monomers, determines the selectivity in spin, and thus a conformational change can switch the spin selectivity.

### Graphical Abstract

Authors are required to submit a graphic entry for the Table of Contents (TOC) that, in conjunction with the manuscript title, should give the reader a representative idea of one of the following: A key structure, reaction, equation, concept, or theorem, etc., that is discussed in the manuscript. Consult the journal's Instructions for Authors for TOC graphic specifications.

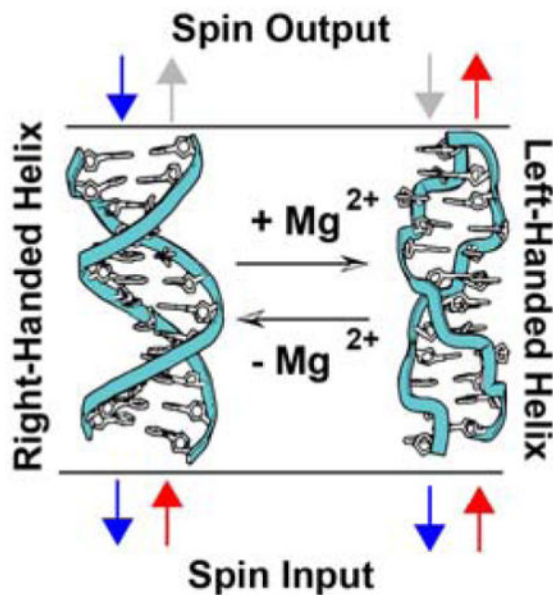
---

\*Corresponding Author: jkbaron@caltech.edu.

#### Notes

The authors declare no competing financial interests.

Supporting Information includes materials and methods, supplementary text, Figs. S1 to S5, Table S1. This material is available free of charge via the Internet at <http://pubs.acs.org>.



DNA-mediated charge transport (DNA CT) is well established in both ground and excited state systems (1). Although theoretical models are still being developed, it is clear that the integrity of the extended  $\pi$ -stack of the aromatic heterocycles, the nucleic acid bases, plays a critical role (2–4): electron donors and acceptors must be electronically well coupled into the  $\pi$ -stack, typically *via* intercalation, and perturbations that distort the  $\pi$ -stack, such as single-base mismatches, abasic sites, base lesions, protein-binding that kinks the double helix, attenuate DNA CT dramatically. This latter characteristic has found practical use in electronic devices and biosensors (5–7).

Recent experimental work in the field of spintronics has raised the intriguing possibility that DNA CT is affected by the inherent spin of the electrons passing through it. The first experiments to show that double stranded DNA (dsDNA) could function as a spin filter were conducted under vacuum, where photoelectrons ejected from a gold surface became spin-polarized after passing through an adsorbed dsDNA monolayer (8). Subsequent conductive AFM measurements showed that the resistance of spin-polarized currents traveling through a thin film of air-dry dsDNA depended on the ratio of spin up versus spin down electrons injected into the film (9). These observations mirror similar experiments that feature other chiral organic molecules within a thin film (10). Because organic molecules display small spin-orbit coupling that would otherwise preclude them from exhibiting spin-selective transport properties, this work has spawned much interest in chirality-induced spin selectivity (CISS) (11–13). Several theories have been offered to account for this effect (14–17). One question of particular interest is whether CISS depends more on the isolated molecular chiral centers or the large-scale macromolecular structures within the films (15).

Owing to its ability to undergo macromolecular conformational changes that affect the helical structure but not the local chirality of the sugar backbone, dsDNA in its native, hydrated state presents a unique opportunity to differentiate between the monomeric and

macromolecular parameters of CISS. Of particular interest is the conformational switching between right-handed B-DNA and left-handed Z-DNA. At high salt concentrations, CG-repeat sequences in the right-handed B-form can flip into a left-handed zigzag Z-form helix (18). Notably, both B-DNA and Z-DNA support efficient DNA CT (19).

We have developed an electrochemical assay to investigate dsDNA-promoted CISS under fluid conditions. Following work by others, (20) our study employs a nickel working electrode capped with a thin (~ 10 nm) layer of gold (Figure 1) (21). Thiol-modified DNA duplexes are then self assembled onto these electrodes, and DNA-binding redox-active probes are added to the electrolyte solution. Magnetizing the nickel surface with a permanent neodymium magnet (0.66 T) generates a spin-polarized current when the potential is poised negative of the formal reduction potential of the DNA-bound probe molecules. The sign of the polarization can be switched by changing the direction of the magnetic field, but its magnitude remains the same. Integrating the Faradaic response of probe-molecule reduction using cyclic voltammetry gives the total number of redox probes reduced, which can be used to quantify the yield of DNA CT under different experimental conditions. Importantly, the redox potentials of all of the probes lie well negative of the potential of zero charge of the working electrode (22). As a result, duplexes within the DNA film line up approximately normal to the gold surface with the magnetic field lines essentially collinear with the helical axes.

Figure 1 shows the results obtained at a densely packed dsDNA film (16 bp duplexes, ~ 40 pmol/cm<sup>2</sup>) using methylene blue (MB) as the redox probe. We have previously shown that MB binds reversibly to DNA monolayers and undergoes a proton-coupled, DNA-mediated 2e<sup>-</sup> reduction to leucomethylene blue (LB) at -220 mV versus AgCl/Ag (23). As can be seen in Figure 1, the yield of MB undergoing electrochemical reduction varies regularly with the orientation of the underlying magnetic field, “up” versus “down”. The change in yield measured by cyclic voltammetry is not large but it is highly reproducible. This effect is fully reversible and can be switched repeatedly by simply flipping over the permanent magnet beneath the nickel surface. The ratio of the integrated reduction peaks of MB varies by 10.9% ± 0.6% upon switching the magnetic field direction (up/down). Increasing the length of the individual DNA helices in these films to 30 bp consistently results in a larger ratio, 15±1%. Importantly, the difference in reduction yield is observed regardless of which direction the nickel is magnetized initially, and the difference persists even when taking multiple scans. There is also no discernable change in the magnetic field effect upon varying the scan rate between 10 mV/s and 20 V/s (21).

The magnetic field dependence of DNA CT was also examined using Nile blue (NB) as a redox probe. NB is covalently bound to DNA, conjugated through a DNA base, and has been used extensively as a covalent redox reporter (Figure 2) (24–26). Self-assembled monolayers of 17 bp thiolated dsDNA with tethered NB (~ 40 pmol/cm<sup>2</sup>) show a change in the integrated reduction peaks of 7±1% upon switching the magnetic field direction. The magnitude of this effect increases with increasing length of dsDNA to 12±2% for 29bp, 16±4% for 43bp, and 29±6% for 60bp oligomers (Fig. S1). There is no measurable effect on the charge-transfer rates with a change in magnetic field direction (27). These data with NB, however, reveal a clear dependence of the yield of DNA CT on magnetic field orientation.

Given the range of possible etiologies for the observed magnetic field effect on the electrochemistry of MB and NB, we carried out a series of control experiments (Figure 2). Monolayers in which MB is adsorbed directly onto the gold-capped nickel electrodes in the absence of DNA show no differences in the reduction yield of MB upon switching the orientation of the magnetic field. Similarly, there is no magnetic field effect on the reduction of MB bound electrostatically to surfaces coated with single stranded DNA. Moreover, capping the nickel electrodes with a thicker (35-nm) gold layer eliminates the magnetic field effects, even for electrodes modified with dsDNA.

Non-intercalative redox probes were also examined for comparison.  $\text{Ru}(\text{NH}_3)_6^{3+}$  binds electrostatically to the phosphate backbone of DNA and undergoes rapid electrochemical reduction to  $\text{Ru}(\text{NH}_3)_6^{2+}$  at dsDNA-modified electrodes (28). Significantly, we find no magnetic field dependence of the  $\text{Ru}(\text{NH}_3)_6^{3+/2+}$  couple, despite its proximity to the chiral macromolecule and likely helical path (Figure 1). We also prepared dsDNA with a covalently bound diazobenzene probe (dabcyl) tethered to the 3'-phosphate near the electrode surface. This arrangement allowed us to monitor simultaneously the direct electrode reduction of dabcyl, which contacts the electrode surface, and the DNA-mediated reduction of MB. There is a significant difference in the up/down yield of MB reduction, but no measurable difference for the dabcyl signal (Fig. S3).

We examined the effect of an intervening single base mismatch in the film (Fig. S4). A mismatch incorporated into dsDNA between the surface and the redox probe decreases the yield of CT to either MB or NB, which shows that the DNA duplex mediates the CT (24); charge migrates *through* the DNA base pair stack. Interestingly, the spin selectivity measured through a mismatch mirrors the magnitude of the effect seen in well-matched duplexes of similar length. This result suggests that when charge is successfully transported through dsDNA with a mismatch, it travels through the entire dsDNA to the probe; the attenuation in CT yield with a mismatch leads to an interruption of some of that CT, but has no effect on spin selectivity.

Combined, these results indicate that: (i) spin polarized currents induced by the underlying magnetic field are needed for spin selectivity in the DNA electrochemistry; (ii) spin selectivity requires double stranded DNA; and (iii) the magnetic field effects are observed only with probes that undergo CT reactions mediated by the DNA duplex.

If the helical structure of dsDNA is responsible for the apparent CISS behavior in these films, it follows that reversing the chirality of the helices would switch the sense of the magnetic field effect. Indeed, this is precisely what we find. Both methylated and unmethylated monolayers of 16bp duplexes featuring  $\text{d}(\text{CG})_8$  repeats were self-assembled onto gold-capped nickel. Circular dichroism confirms that DNA oligomers containing 5-methylcytosine,  $\text{d}(\text{mCG})_8$  undergo a B-to-Z transition in the presence of 10 mM  $\text{MgCl}_2$ , while the unmethylated analog,  $\text{d}(\text{CG})_8$  remains B-form (Fig. S5); methylated Z-DNA reverts back to B-DNA upon rinsing away the  $\text{MgCl}_2$  (18,29,30). Previous work has shown that MB intercalates into both B- and Z-DNA and undergoes DNA-mediated reduction in the presence of 10 mM  $\text{MgCl}_2$  (19).

We carried out the electrochemistry to examine B- and Z-form helices on a multiplexed chip (24) consisting of 16 separate gold-capped nickel regions that allowed for the simultaneous comparison of four distinct monolayers under the identical magnetic field (Figure 3). In the absence of  $\text{MgCl}_2$ , both methylated and unmethylated DNA films show the same favored magnetization direction for a higher yield of MB reduction (up/down ratio =  $18 \pm 3\%$ ). Upon addition of 10 mM  $\text{MgCl}_2$ , the unmethylated films show no change in behavior, but the methylated films switch which magnetic field direction promotes the higher yield of MB reduction (up/down ratio =  $-9 \pm 2\%$ ). Replacing the buffer with one that lacks  $\text{MgCl}_2$  reverts the structure from Z- to B-form and restores the original characteristics, yielding again an up/down ratio of  $18 \pm 2\%$  for both films.

In addition to functioning as a magnetic field diode, switching between B- and Z-form dsDNA gives a difference in the magnitude of DNA CISS; normalized to the yield of electrochemically active MB and with the assumption that 10 mM  $\text{MgCl}_2$  results in complete conversion of surface-bound DNA to Z-form, B-DNA appears to have an approximately 50% larger spin selectivity than Z-DNA. This change in magnitude of spin selectivity correlates well with the change in pitch between B-DNA and Z-DNA (3.32 nm and 4.56 nm respectively) but may result from other differences between the two forms (such as the greater  $\pi$ -stacking in the B- versus Z-form) (18,29,30). These data suggest that the charge is moving through the duplex along a helical path, because a charge moving in a fully delocalized  $\pi$ -stacked column would not be able to interact with the handedness of the macromolecule; helical transport among delocalized domains of a few base pairs is possible.

The CISS measured in these experiments is significantly larger than expected for molecules that lack large spin-orbit coupling. Calculating the energy difference between the two electron spins at the surface of fully magnetized nickel ( $\sim 0.6$  T) yields a gap ( $\mu_B g B \approx 1 \text{ cm}^{-1}$ ) far lower than  $k_B T$  at ambient temperature. Several theoretical models have been proffered to rationalize the large CISS exhibited by chiral organic films (16,17, 31–35). Aspects of each of these models can be used to understand our data. In addition, it is worthwhile to consider other factors not currently included in these models that are important in the context of DNA CT, such as the large polarizability of the  $\pi$ -stack in dsDNA (36) or the delocalization of domains across multiple adjacent nucleotides (37,38).

Our experiments thus demonstrate that magnetic fields can affect the flow of electrons through native, hydrated dsDNA. Significantly, our data show that electrochemically generated DNA CISS is observed only at films containing duplex DNA and with redox probes intercalated into the  $\pi$ -stack that undergo DNA-mediated CT. Magnetic field effects are not observed with redox reporters bound electrostatically to the DNA duplex nor with tethered reporters that contact the surface directly. It is not simply the electrostatic helical field that is responsible for the spin-selectivity. Nor is it simply the chiral centers on the DNA; redox reporters bound to single stranded DNA do not show magnetic field effects. As with DNA CT, the extended  $\pi$ -stack appears to play the crucial role: reversing the handedness of the helix in the films generates a diode-like spin-filtering response. It is interesting to consider how conformational changes such as that between B- and Z-DNA might be utilized as a diode in organic spintronics, indeed, how this spin filtering might be

applied in practical devices. Finally, it is intriguing to consider whether Nature exploits this helix-dependent spin selectivity of DNA in some context.

## Supplementary Material

Refer to Web version on PubMed Central for supplementary material.

## Acknowledgments

We are grateful to the NIH (GM61077) and the Moore Foundation for their financial support. TJZ is also an NSF GRFP fellow (DGE-1144469). We thank Dr. Natalie Muren for discussions. We thank John Abendroth, Professor Paul Weiss, Elizabeth O'Brien, and Philip Bartels for providing gold-capped nickel surfaces.

## References

1. Genereux JC, Barton JK. *Chem Rev.* 2010; 110:1642–1662. [PubMed: 20214403]
2. Guo X, Gorodetsky AA, Hone J, Barton JK, Nuckolls C. *Nat Nanotech.* 2008; 3:163–167.
3. Muren NB, Olmon ED, Barton JK. *Phys Chem Chem Phys.* 2012; 14:13754–13771. [PubMed: 22850865]
4. Berlin YA, Voityuk AA, Ratner MA. *ACS Nano.* 2012; 6:8216. [PubMed: 22901272]
5. Porath D, Cuniberti G, Felice RD. *Top Curr Chem.* 2004; 237:183.
6. Drummond TG, Hill MG, Barton JK. *Nature Biotech.* 2003; 21:6475.
7. Barton, JK.; Furst, AL.; Grodick, MA. *DNA in Supramolecular Chemistry and Nanotechnology.* Stults, E.; Clever, GH., editors. Wiley; 2015.
8. Gohler B, Hamelbeck V, Markus TZ, Kettner M, Hanne GF, Vager Z, Naaman R, Zacharias H. *Science.* 2011; 331:894. [PubMed: 21330541]
9. Xie Z, Markus TZ, Cohen SR, Vager Z, Gutierrez R, Naaman R. *Nano Lett.* 2011; 11:4652–5644. [PubMed: 21961931]
10. Sun D, Ehrenfreund E, Varedny ZV. *Chem Commun.* 2014; 50:1781–1793.
11. Michaeli K, Kantor-Uriel N, Naaman R, Waldeck DH. *Chem Soc Rev.* 2016 in press.
12. Mondal PC, Kantor-Uriel N, Mathew SP, Tassinari F, Fontanesi C, Naaman R. *Adv Material.* 2015; 27:1924–1927.
13. Dor OB, Yochelis S, Mathew SP, Naaman R, Paltiel Y. *Nat Comm.* 2013; 4:2256.
14. Gutierrez R, Diaz E, Naaman R, Cuniberti G. *Phys Rev B.* 2012; 85:081404.
15. Naaman R, Waldeck DH. *Ann Rev Phys Chem.* 2015; 66:263. [PubMed: 25622190]
16. Guo A-M, Sun Q-F. *Phys Rev Lett.* 2012; 108:218102. [PubMed: 23003304]
17. Medina E, Lopez F, Ratner MA, Mujica V. *Eur Phys Lett.* 2012; 99:17006.
18. Saenger, W. *Principles of nucleic acid structure.* Springer-Verlag; New York: 1984.
19. Boon EM, Barton JK. *Bioconjugate Chem.* 2003; 14:1140–1147.
20. Mondal PC, Fontanesi C, Waldeck DH, Naaman R. *ACS Nano.* 2015; 9:3377–3384. [PubMed: 25752750]
21. See Supplementary Materials for additional Figures.
22. Kelley SO, Barton JK, Jackson NM, McPherson LD, Potter AB, Spain EM, Allen MJ, Hill MG. *Langmuir.* 1998; 14:6781.
23. Kelley SO, Barton JK, Jackson N, Hill MG. *Bioconjugate Chem.* 1997; 8:31–37.
24. Slinker JD, Muren NB, Renfrew SE, Barton JK. *Nat Chem.* 2011; 3:228–233. [PubMed: 21336329]
25. Gorodetsky AA, Hammond WJ, Hill MG, Slowinski K, Barton JK. *Langmuir.* 2008; 24:14282–14288. [PubMed: 19053641]
26. Muren NB, Barton JK. *J Am Chem Soc.* 2013; 135:16632–40. [PubMed: 24164112]

27. To test for effects of magnetic field on the CT rate, we varied the scan rate from 50 mV/s to 20 V/s (Fig. S2); we see no difference in the cathodic/anodic peak splittings when the magnetic field direction is switched, suggesting that there is no measurable effect on the charge-transfer rates with a change in magnetic field direction. We stress however that previous work has shown that in these electrochemical experiments the DNA CT rates are limited by tunneling through the alkanethiol linker, ( Drummond TG, Hill MG, Barton JK. *J Am Chem Soc.* 2004; 126:15010. [PubMed: 15547981] ) not transport through the DNA, so small changes in the inherent tunneling efficiencies of oppositely polarized currents through the  $\pi$ -stack would not be accessible electrochemically.
28. Yu H-Z, Luo C-Y, Sankar CG, Sen D. *Anal Chem.* 2003; 75:3902. [PubMed: 14572060]
29. Hartmann B, Lavery R. *Q Rev Biophys.* 1996; 29:309–368. [PubMed: 9080547]
30. Wang AHJ, Quigley GJ, Kolpak FJ, Crawford JL, Van Boom JH, Van Der Marel GA, Rich A. *Nature.* 1979; 282:680–686. [PubMed: 514347]
31. Gutierrez R, Diaz E, Naaman R, Cuniberti G. *Phys Rev B.* 2012; 85:081404.
32. Gutierrez R, Diaz E, Gaul C, Brumme T, Dominguez-Adame F, Cuniberti G. *J Phys Chem C.* 2013; 117:22276–22284.
33. Guo AM, Sun QF. *Proc Natl Acad Sci.* 2014; 111:11658–11662. [PubMed: 25071198]
34. Gersten J, Kaasbjerg K, Nitzan A. *J Chem Phys.* 2013; 139:114111. [PubMed: 24070283]
35. Michaeli K, Naaman R. *arXiv.* 2016:1512.03435v2.
36. Williams TT, Barton JK. *J Am Chem Soc.* 2002; 6:1840–1841.
37. O’Neil MA, Barton JK. *J Am Chem Soc.* 2004; 126:11471. [PubMed: 15366893]
38. Xiang L, Palma JL, Bruot C, Mujhica V, Ratner MA, Tao N. *Nature Chem.* 2015; 7:221–226. [PubMed: 25698331]

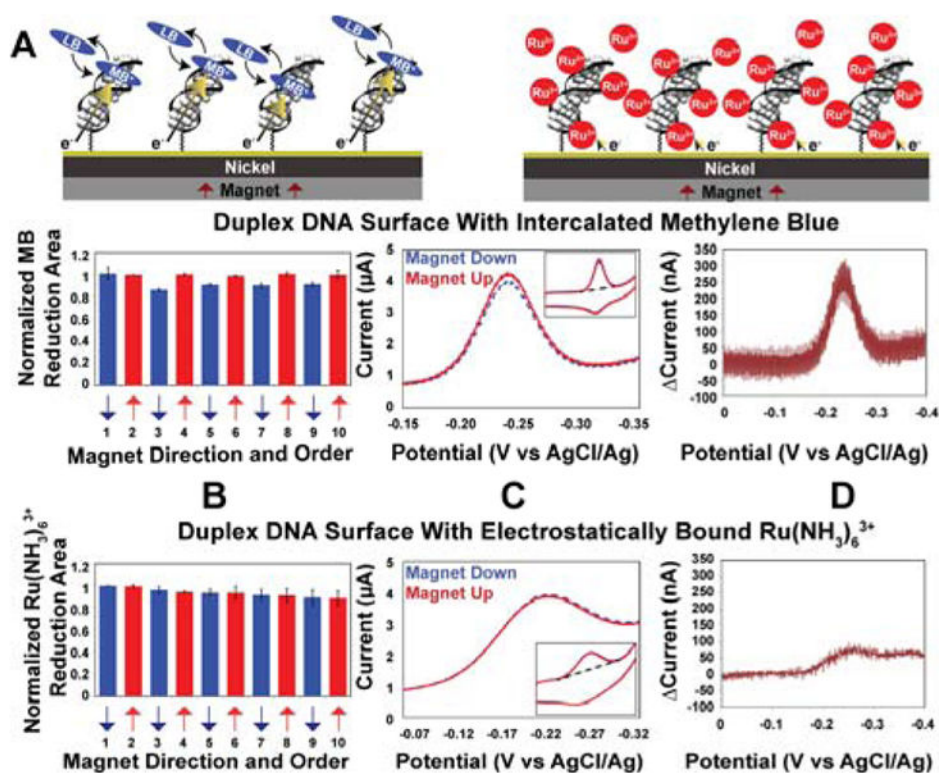


**Figure 1. Cyclic voltammetry on electrodes modified with 16 bp dsDNA**

**A.** Illustration of the dsDNA modified electrodes with 1  $\mu\text{M}$  methylene blue (MB) (left) or 10  $\mu\text{M}$   $\text{Ru}(\text{NH}_3)_6^{3+}$  (right). **B.** For intercalated MB (above) and electrostatically bound  $\text{Ru}(\text{NH}_3)_6^{3+}$  (below) reduction yield upon switching the magnetic field direction. Data were normalized to the first scan with the magnetic field pointing up. **C.** Representative cyclic voltammograms with the magnet up (red, solid) and magnet down (blue, dotted). **D.** Difference plot showing the current when the magnetic field is pointing up minus the current when the magnetic field is pointing down. The  $\text{Ru}(\text{NH}_3)_6^{3+}$  experiments were typically done following MB experiments on the same surface.

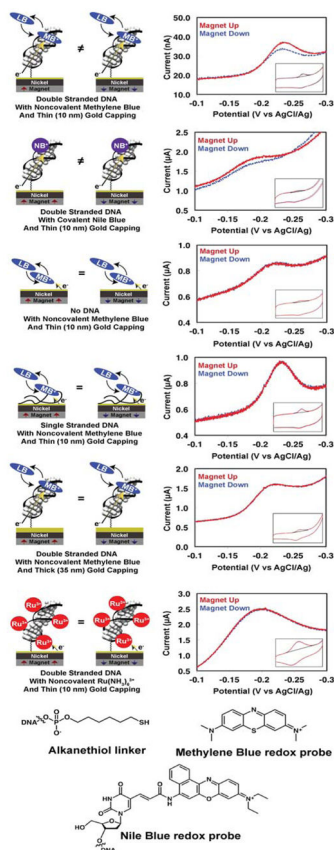


**Figure 2. Representative cyclic voltammetry data for various assemblies of DNA-modified electrodes**

29 bp dsDNA or ssDNA was tethered to a gold-capped nickel surface with an alkanethiol linker. Insets display the full cyclic voltammogram, while the larger plot displayed is centered around the reduction peak of the redox probe.

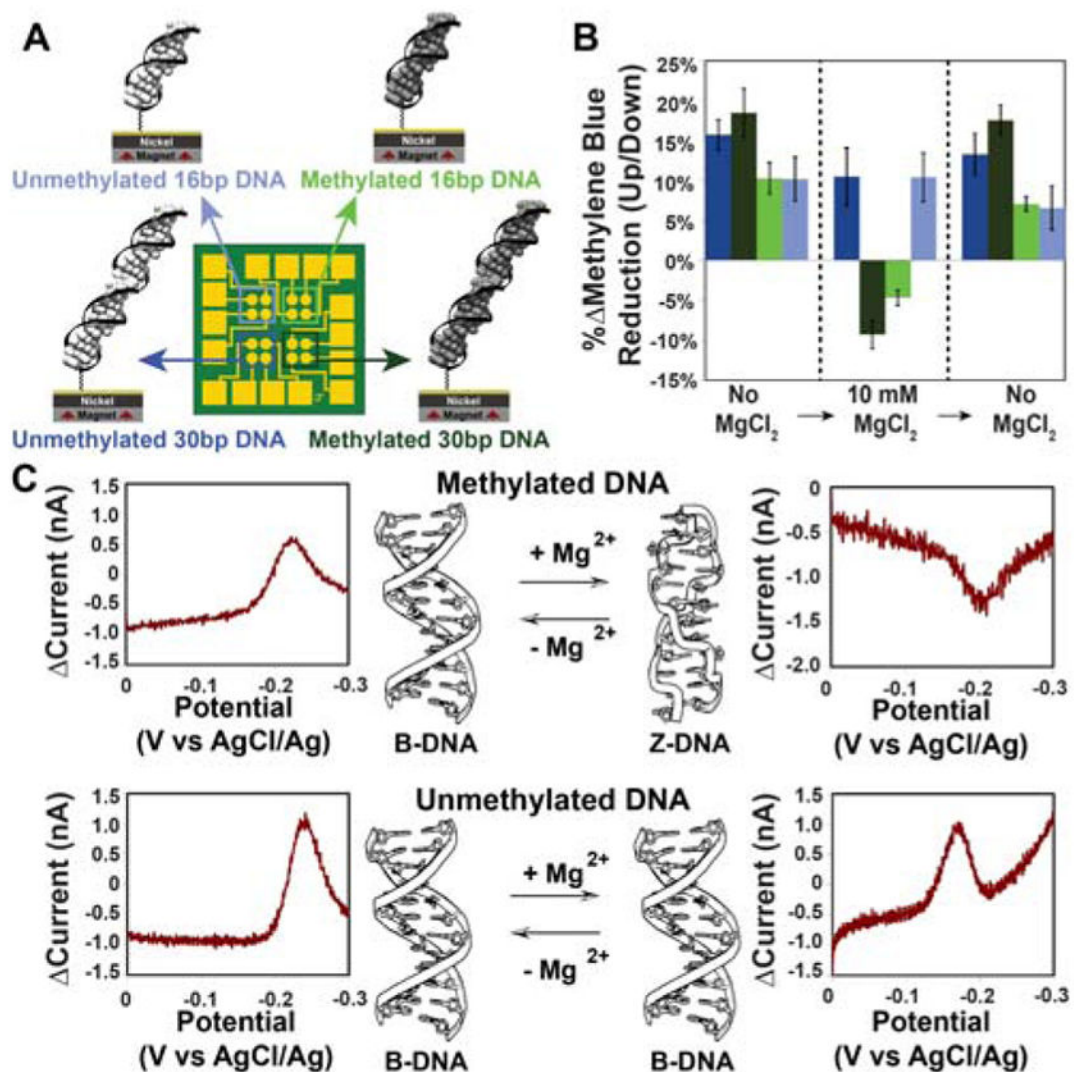


**Figure 3. Switching of methylated and unmethylated dsDNA measured on a single multiplexed chip**

**A.** A multiplexed chip was prepared with 4 distinct monolayers. **B.** Summary of cyclic voltammetry data for the two magnetizations were collected for all four quadrants with no  $MgCl_2$ , then with 10 mM  $MgCl_2$ , then after washing away the  $MgCl_2$ . Each bar represents a minimum of 4 separate electrode surfaces. **C.** Representative data for 30 bp (top) methylated  $d(mCG)_{15}$  and (bottom) unmethylated  $d(CG)_{15}$  Data are plotted as the difference in current for a reductive sweep when the magnetic field is pointing up minus the current when the magnetic field pointing down.